Journal of ELECTRONIC MATERIALS, Vol. 48, No. 11, 2019
https://doi.org/10.1007/s11664-019-07542-7

Ultrafine SnO_2 Nanoparticles Encapsulated in High-Conductivity Graphited Carbon Nanotubes As Anodes for High Electrochemistry Performance Lithium-Ion Batteries

JI YU ,[1,2] HAI-YAN WEI,[1] ZHEN-YU YANG,[1] and JIAN-XIN CAI[1]

1.—College of Chemistry, Nanchang University, Nanchang 330031, China. 2.—e-mail: yuji@ncu.edu.cn

Efficient use of tin-based composites plays an active role in energy-storage systems due to their high theoretical capacity and environmental benignity. But, large volume expansion during Li-ion insertion/extraction and undesirable aggregation of tin particles greatly limit the commercial application of Sn-based anodes. In this work, the SnO_2 nanoparticles encapsulated in high-conductivity graphited carbon nanotubes (gCNTs) had been designed and synthesized by a facile wet chemical method, in which SnO_2 nanoparticles with a diameter of 3–6 nm were protected by gCNT nano-containers. With the increase of graphiting temperature from 2400°C to 2800°C, more SnO_2 nanoparticles were encapsulated in the gCNT containers instead of being attached to the outer surface. The SnO_2/gCNT composites showed an excellent Li-ion storage capability and long cycling stability. The initial discharge capacities of the SnO_2-gCNT composites were 1455 mAh g^{-1}, and kept final capacity of 383 mAh g^{-1} after 620 cycles at 4 A g^{-1}. Furthermore, this work provides a simple and effective strategy to prepare the ultrafine nanoparticles encapsulated in high-conductivity gCNTs for Li-ion batteries.

Key words: Tin oxide, graphited carbon nanotubes, Li-ion batteries, anode material

INTRODUCTION

The increasing emission of greenhouse gases, fossil fuel supply constraint and concern on climate change have attracted a mass of public awareness of the development of green technology, such as hybrid electric vehicles (HEVs) and electric vehicles (EVs). Compared with various energy storage systems, lithium ion batteries (LIBs) now present the best performance to meet the application demands because of their high gravimetric and volumetric energy density, long cycle life and low self-discharge rate. But, LIBs are still confronted with a major technical challenge to increase the capacity, rate capability and durability to meet the steadily increasing energy density demands for large-size applications.

The following successor of LIB anode materials include tin, silicon, polymers and transition-metal oxides.[1–4] Among these, tin,[5] tin alloys[6] and tin oxide[7–9] are deemed good long-term choices because of their high theoretical capacity, environmental benignity and extensive availability.[10–15] Many works are devoted to preparing different shapes of SnO_2, such as nanorods,[16,17] nanosheets,[18,19] flower-like [20,21] and hollow structures,[22–24] or incorporating with high conductivity materials such as carbon nanotubes,[9,22] carbon fibers,[25,26] graphene nanosheets[27,28] and carbon.[29–31] But it is regrettable that some shortcomings limit the commercial application of SnO_2 anodes such as large volume expansion that occurs during Li-ion insertion/extraction (> 300%), capacity deterioration, undesirable aggregation of tin particles and the formation

(Received June 11, 2019; accepted August 9, 2019; published online August 22, 2019)

of thick solid electrolyte interphase (SEI) during cycling.[16]

Up to now, SnO_2/C-based composites have been proved to be effective structures to prolong the cycle life of the SnO_2 owing to the excellent electrical conductivity of C and its natural buffering role, [25–27] which can help to restrict the volume expansion of SnO_2 during the charge–discharge process.[16] Dongdong Liu et al.[32] developed SnO_2/graphene sphere-like composites in polypyrrole nanofilm. The skeleton-structured SnO_2/graphene spheres can display a specific discharge capacity of 1140 mAh g^{-1} after 120 cycles under a current density of 100 mA g^{-1}. Seung Ho Choi et al.[33] discovered SnO_2/CNTs composite microspheres with perforated and filled structures had an initial discharge capacity of 1108 mAh g^{-1}, and 590 mAh g^{-1} after 250 cycles at the current density of 1.5 A g^{-1}. Rengcheng Jin et al. [34] designed and fabricated SnO_2 quantum dots anchored on amorphous carbon coated with multi-walled carbon nanotubes (CNTs@C@SnO_2) by a solvothermal process accompanied by a high temperature calcination treatment. At the current density of 5 A g^{-1}, the capacities of 515 mAh g^{-1} are achieved after 300 cycles. Furthermore, compared to SnO_2, SnO_2/C-based composites show a larger specific surface area which is very helpful for increasing the chance of lithium-ion transition to the active substance.[35]

Herein, we report a facile strategy to synthesize SnO_2 nanoparticles encapsulated in graphited carbon nanotubes as an advanced anode material for high-performance LIBs. The SnO_2 nanoparticles are 3–6 nm in diameter and wrapped by graphited carbon nanotubes which act as a container to protect SnO_2 from the damage of volume expansion during the charge–discharge process. As expected, the composites display a superior Li-ion storage performance with large reversible capacity, high coulombic efficiency, excellent cyclic performance, and rate capability.

EXPERIMENTAL

Treatment of Raw Carbon Nanotubes

Raw CNTs were supplied by Nanjing Ji Bin Nanometer Science and Technology Co., Ltd. (Nanjing, China) and used as received. The inner and outer diameters of the raw CNTs are about 20–70 nm and 80–100 nm estimated by TEM (JEM-200CX, operated at 200 kV). To get more SnO_2 nanoparticles into the CNTs, the raw CNTs were treated before using. The steps are described as follows: firstly, the raw CNTs were dispersed in distilled water by an ultrasonic wave for half an hour and then soaked in 30% hydrogen peroxide for 5 h.[36] Then the raw CNTs were refluxed in nitric acid solution (20 wt.%) at 100°C for another 5 h, and then washed by water and ethanol until neutral and dried at 80°C. Usually, the graphitization degree of newly prepared CNTs is low because the temperature of the preparation process is only about 1000°C. Therefore, the treated-CNTs (tCNTs) were heated in graphitization furnace under 2400°C, 2600°C and 2800°C for 2 h with a heating rate of 10°C min^{-1} in nitrogen atmosphere to increase graphitization, the products were signed as gCNTs-24t, gCNTs-26t and gCNTs-28t.

Synthesis of SnO_2 Encapsulated in Graphited Carbon Nanotubes

In the beginning, 0.96 g $SnCl_2{\cdot}2H_2O$ was dispersed in 100 mL distilled water and stirred for 0.5 h to get a homogeneous $SnCl_2$ solution. About 0.1 g graphited carbon nanotubes were added into a flask and then the air in the flask was moved by a vacuum pump. After that, $SnCl_2$ solution was injected slowly and stirred by a magnetic stirrer. The reaction system was maintained at room temperature and evacuated every 2 h to get more tin ions into gCNTs. The total filling time was from 24 h to 100 h. Finally, the above solution was refluxed 3 h at 140°C, and then solid products were collected and calcined at 400°C in argon for 2 h to get the SnO_2/gCNTs composites, the final products were signed as S-gCNTs-yyt-xxxh (xxx = filling time).

Characterization

X-ray diffraction was collected using a Rigaku D/Max-IIIA x-ray diffractometer with Cu Kα radiation (λ = 1.5418 Å). Morphology and structure of the samples were examined by scanning electron microscopy (SEM, FEI Quanta 200F) and transmission electron microscopy (TEM, JEM-200CX). X-ray photoelectron spectroscopy (XPS) spectra were collected on an AXIS-Ultra instrument from Kratos Analytical with a monochromatic Al Kα radiation (225 W, 15 mA, and 15 kV) and low-energy electron flooding for charge reimbursement. Thermogravimetric analysis (TGA) was carried out on a thermogravimetric-differential scanning calorimetry (TG-DSC) analyzer (Mettler-Toledo, TGA/DSCI-LF-1100) from room temperature to 900°C in air with a temperature ramp of 10°C min^{-1}.

Electrochemical Measurements

Electrochemical tests were carried out using CR2025 half cells with lithium foil as the counter electrode and Celgard 2400 films as a separator. The active materials (for example, gCNTs), acetylene black, and polyvinylidene difluoride (PVDF) solution in N-methyl-2-pyrrolidine (NMP) were mixed with a weight ratio of 84:10:6. The slurry was coated on Cu foil and cut into rounds with a diameter of 16 mm. Electrolyte was a 1 M $LiPF_6$ solution in the EC/DEC/DMC mixture (1:1:1 in volume). The cells were assembled in a glove box filled with pure argon (99.999%) and then aged for 12 h at room temperature before the galvanostatic discharge–charge

test (on NEWARE cell test system, China) between 0.01 V and 2.5 V (versus Li/Li$^+$). Electrochemical impedance spectra (EIS) data were recorded by the electrochemical workstation system IM6ex (Zahner, Germany).

RESULTS AND DISCUSSION

Structure Analysis

The XRD curves of the gCNTs calcined at a different temperatures of 2400°C, 2600°C and 2800°C and tCNTs are shown in Fig. 1. All samples displayed three major diffraction peaks at 2θ = 26.6, 43.4 and 46.3. These peaks can be indexed to the planes of graphite (JCPDS No. 75-2078)[37] and the diffraction peaks became sharper and higher due to the increase of calcined temperature, which means the increase of graphitization degree of CNTs.

TEM was used to study the morphology and structures of the as-synthesized products. As shown in Fig. 2, most of the SnO_2 nanoparticles entered into the CNTs, but there was small difference among four samples. For Fig. 2a, many hydroxyl and carboxyl groups adhered to the outer surface of CNTs after being treated by hydrogen peroxide and nitric acid, which makes Sn^{2+} ions more easily adsorbed on the outer surface of CNTs, and finally formed SnO_2 . These adsorbed SnO_2 particles were harder to remove by washing with distilled water. But after calcining at high temperature (from 2400°C to 2800°C), the hydrophilic groups on the surface of CNTs were significantly reduced, which results in the decrease of SnO_2 on the outer surface of CNTs. The higher the calcined temperature, the less SnO_2 there is on the outer surface of CNTs, as seen in Fig. 2b, c and d.

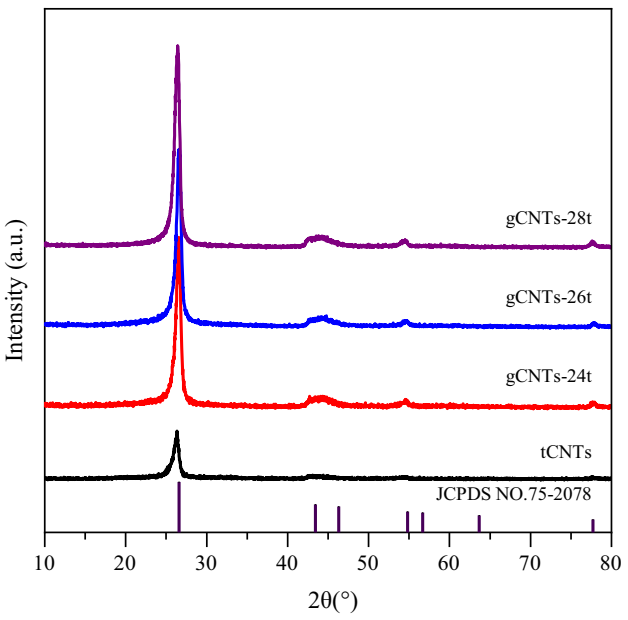

Fig. 1. XRD curves of the tCNTs and gCNTs calcined at different temperature.

XRD curves of the samples with different filling times are shown in Fig. 3a. It was obvious that five major diffraction peaks at 2θ = 26.7°, 34.0°, 38.2°, 51.5° and 66.0° can be indexed to the (110), (101), (200), (211) and (112) planes of tetragonal rutile SnO_2 (JCPDS No. 41-1445), and no other impurity diffraction peaks were found, which meant all samples were pure SnO_2.

Thermal gravimetric (TG) curves of S-gCNTs-28t-24h, S-gCNTs-28t-64h and S-gCNTs-28t-100h showed one-step weight-loss below 900°C caused by the combustion of graphited CNTs, as shown in Fig. 3b. The weight-loss was 52.1wt.%, 44.4wt.% and 39.4wt.% corresponding to the filling time form 24 h to 100 h. A calculated content of SnO_2 nanoparticles in composites was 47.9wt.%, 55.6wt.% and 60.6wt.%, which significantly increased with the increase of the filling time. The higher content of SnO_2 nanoparticles in the composites will lead to a higher discharge capacity, as shown in Fig. 4.

X-ray photoelectron spectroscopy (XPS) was used to detect the chemical composition of the surface of the sample S-gCNTs-28t-100h. XPS full survey clearly showed the presence of Sn, C, and O elements shown in Fig. 3c. The high resolution spectrum for the Sn element presented in Fig. 3d showed two characteristic peaks for Sn^{4+} around 487 eV (Sn $3d_{5/2}$) and 496 eV (Sn $3d_{3/2}$). The XPS results are good agreement with the XRD results and show the successful preparation of SnO_2-gCNTs composites.

Morphology Analysis

Figure 5a, b and c displayed the S-gCNTs-28t composites with different filling times. The pictures clearly showed that most of SnO_2 nanoparticles filled inside the CNTs, and only a few adsorbed on the outer surface. With the increase of the filling time, the filling-degree of the CNTs also increased, which was consistent with the results of TG (Fig. 3b). The huge volume expansion and shrinking of SnO_2 during the charge–discharge process can be limited in the interior of CNTs and result in good electrochemistry performance. Figure 5d was HRTEM image of S-gCNTs-28t-100h, the image displayed a well-crystallized SnO_2 nanoparticles with the size of 3–6 nm in diameter embedded in the tube. The d-spacing determined from the HRTEM is 0.33 nm, which can be indexed to the (110) face of tetragonal SnO_2, as shown in Fig. 5e. Furthermore, as shown in Fig. 5d, SnO_2 nanoparticles had vague interfaces with the CNTs indicating that the Sn-O-C possibly formed some metastable phases in the boundary between SnO_2 and CNTs.[38] The ring-like selected-area electron diffraction (SAED) pattern was showed in Fig. 5f. The bright diffraction rings indicated the presence of polycrystalline SnO_2 nanoparticles and can be indexed to (110), (101),

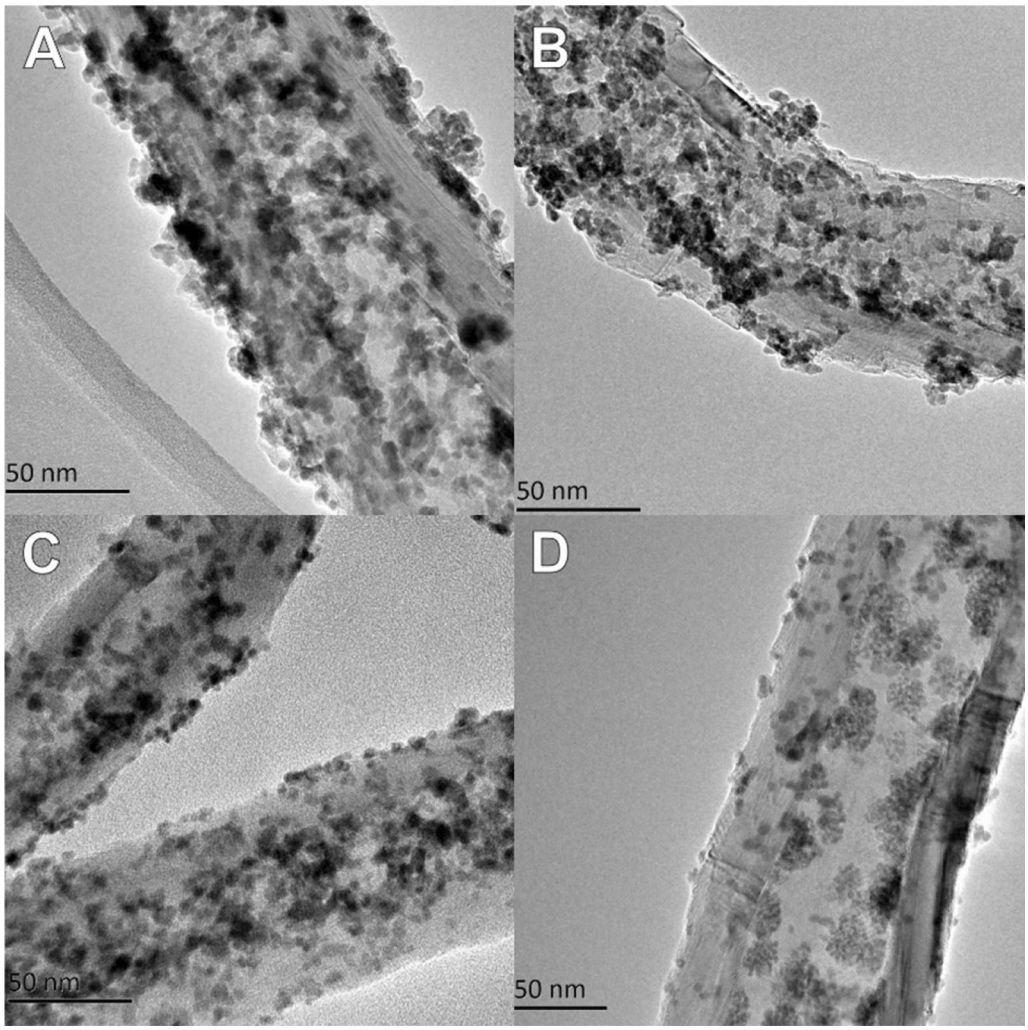

Fig. 2. TEM images of (a) S-tCNTs-100h, (b) S-gCNTs-24t-100h, (c) S-gCNTs-26t-100h and (d) S-gCNTs-28t-100h.

(200), (211), and (112) planes of rutile SnO_2 from the inside out.

Electrochemical Performance Analysis

The first three charge–discharge curves of the sample S-gCNTs-28t-24h, S-gCNTs-28t-64h and S-gCNTs-28t-100h are shown in Fig. 4. It was revealed that Li^+ would react with both SnO_2 and CNTs in the composites and, as a result, the active materials delivered a high initial Li^+ storage capacity. As shown in Fig. 4, the first discharge capacities were 756 mAh g^{-1}, 1114 mAh g^{-1}, and 1455 mAh g^{-1} for the three samples at the current density of 70 mA g^{-1}. The discharge capacities of these samples were much higher than the theoretic capacity of graphite (372 mAh g^{-1}). Sample S-gCNTs-28t-100h displayed the highest initial irreversible capacity loss than the other two samples, similar to that reported in the literature.[38–42] The irreversible capacity loss is mainly ascribed to the electrolyte disintegration and the formation SEI films on the fragmented CNTs surfaces with an increased specific surface area because of solution immersion.[43]

The rate performance of the samples S-gCNTs-28t-24h, S-gCNTs-28t-64h, S-gCNTs-28t-100h and gCNTs are shown in Fig. 6a. Although the discharge capacities declined with the crescendo of the applied current density, all the S-gCNTs composites still showed a superior reversible capacity than gCNTs. The discharge capacity of samples S-gCNTs-28t-100h, S-gCNTs-28t-64h and S-gCNTs-28t-24h remained 631 mAh g^{-1}, 520 mAh g^{-1} and 421 mAh g^{-1} after working at a current density of 0.4 A g^{-1} for ten cycles, higher than that of gCNTs (or graphite). Generally, the discharge capacity of the samples would decrease quickly when the current density increased. It is impressive that all S-gCNT composites displayed excellent rate performance. For example, the sample S-gCNTs-28t-100h could still reserve a discharge capacity of 520 mAh g^{-1} and 386 mAh g^{-1} under the current density of 0.8 A g^{-1} and 4 A g^{-1}. Even under a large

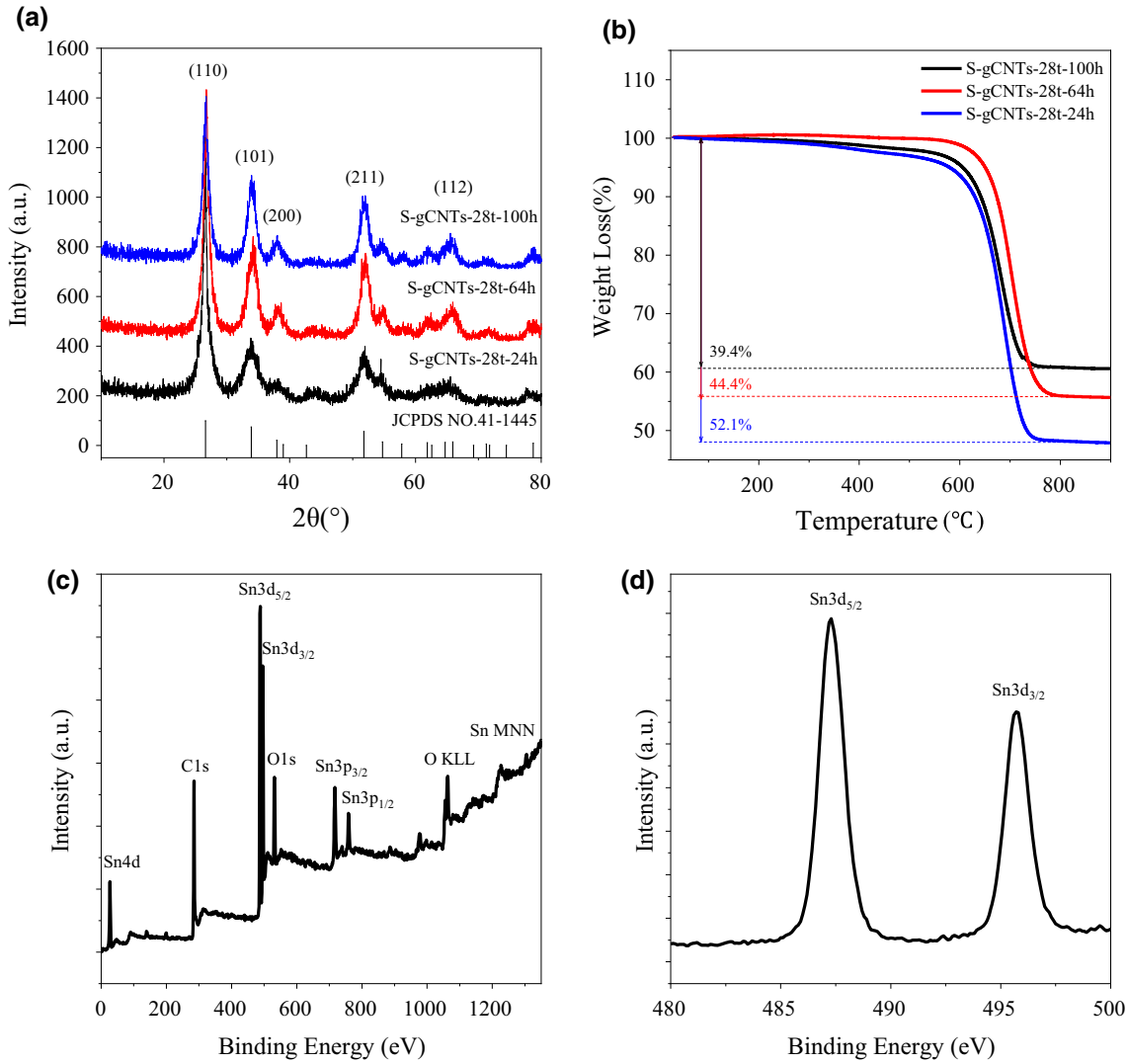

Fig. 3. (a) XRD and (b) TG curves of the samples S-gCNTs-28t-24h, S-gCNTs-28t-64h and S-gCNTs-28t-100h; (c) XPS full survey and (d) high-resolution XPS surveys of Sn 3d regions of S-gCNTs-28t-100h.

current density of 8 A g^{-1}, the composites still held a satisfactory reversible discharge capacity of 308 mAh g^{-1} and when the current density decreased to 0.4 mA g^{-1}, the discharge capacity of the S-gCNTs-28t-100h could restore the original capacity and maintain a capacity of 561 mAh g^{-1} at the 50th cycle. The other two composites displayed a similar behavior as sample S-gCNTs-28t-100h, but lower discharge capacity because of the low content of SnO_2 in the composites. The excellent ability of restoring and maintaining the discharge capacity can be attributed to the stable core–shell structure of the composites.[44] Graphited CNTs with ordered and unbreakable structure can limit the immensity and reduplicative volume change of SnO_2 and offer a good electric conducting network for the anode in the same time during the process of charge–discharge.[39,40]

As shown in Fig. 6b, after a dramatically decreasing during the first nine cycles, sample S-gCNTs-28t-100h delivered a reversible capacity about 383 mAh g^{-1} and hardly decayed after 620 cycles at a current density of 4 A g^{-1}. Sample S-gCNTs-28t-64h and S-gCNTs-28t-24h have a similar electrochemical behavior as sample S-gCNTs-28t-100h, but lower discharge capacity because of the lower content of SnO_2 in the composites mentioned above. For comparison, the discharge capacities of gCNTs and SnO_2/CNTs mixtures (a mixture of SnO_2 and CNTs mixed by a mechanical method) were investigated too. The gCNTs owned discharge capacity of 1410 mAh g^{-1} at the first cycle, but it dropped to 52 mAh g^{-1} after 620 cycles. The performance of SnO_2/CNTs mixtures was good in the first few cycles. It has as same high initial discharge capacity of 1428 mAh g^{-1} as gCNTs, but it suffered from rapid capacity decay even in the first 200 cycles just displayed in Fig. 6b. The results described above show that only an organic combination of two materials can achieve good electrochemistry

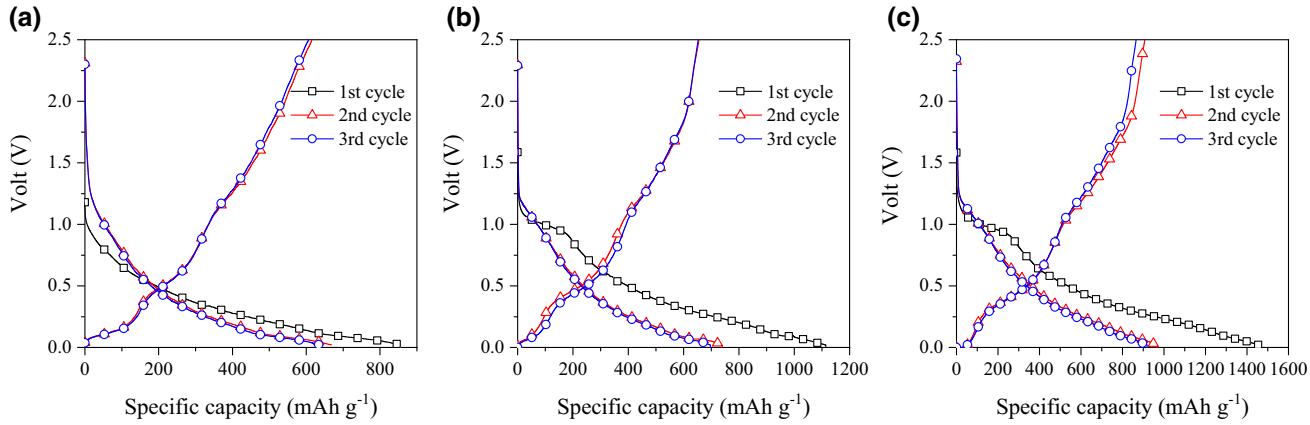

Fig. 4. First three charge/discharge profiles of the samples S-gCNTs-28t-24h (a), S-gCNTs-28t-64h (b) and S-gCNTs-28t-100h (c) at a current density of 70 mA g^{-1} between 0.01 V and 3.0 V.

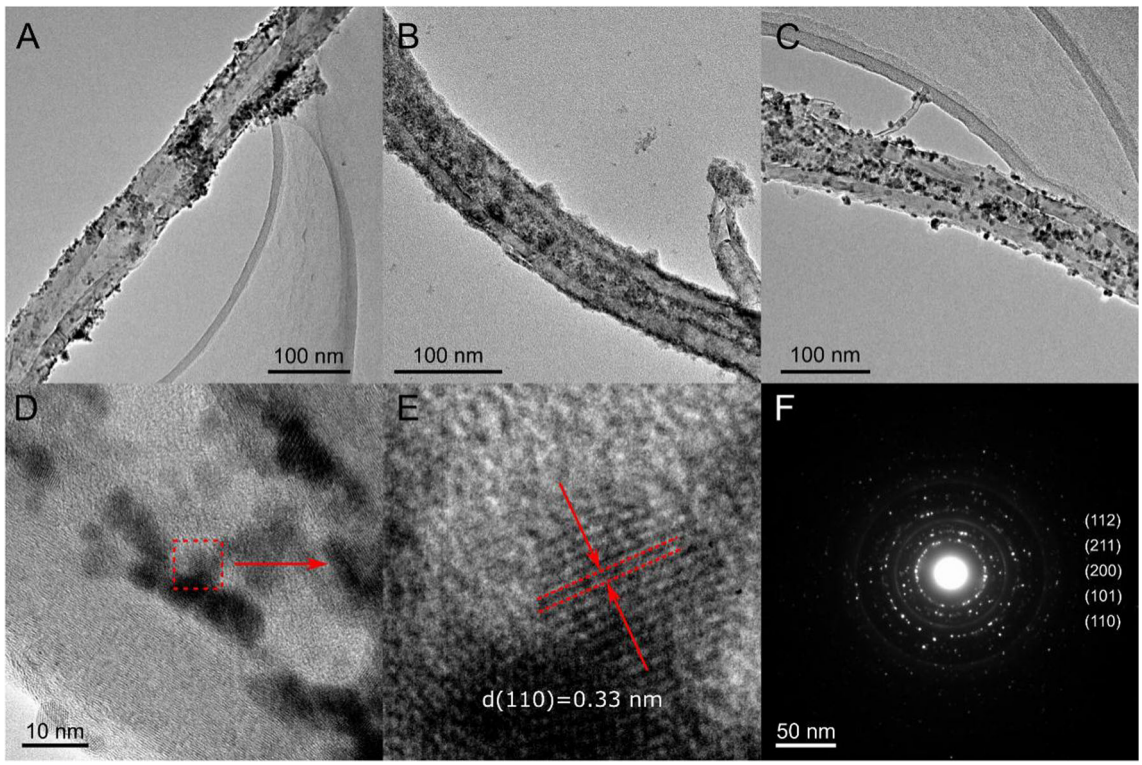

Fig. 5. TEM images of S-gCNTs-28t-24h (a), S-gCNTs-28t-64h (b) and S-gCNTs-28t-100h (c); HRTEM images (d, e) and SAED spectral graph (f) of S-gCNTs-28t-100h.

performance, just like the gCNTs-28t-100 h. Moreover, the gCNTs-28t-100 h had a much higher coulombic efficiency than that of other samples indicating the fact that Li-ion can migrate more easily in S-gCNTs-28t-100h, which was confirmed by further investigation.

Impedance analysis was used to analyze the change in resistance of the composites and the results were shown in Fig. 7a and b. The arc in resistance is attributed to the charge-transfer resistance.[45] It can be seen from Fig. 7a that high graphiting temperature will lead to a decrease of charge-transfer resistance because of the increase of the level of order of CNTs. Moreover, the charge-transfer resistance gradually decreased with the increase in filling time, as shown in Fig. 7b. A longer reaction time made more SnO_2 nanoparticles enter the cavity of CNTs. As a result, the contact between the SnO_2 nanoparticles and SnO_2 nanoparticles or CNTs become closer that led to the decrease of charge-transfer resistance and the excellent rate performance of the composites.

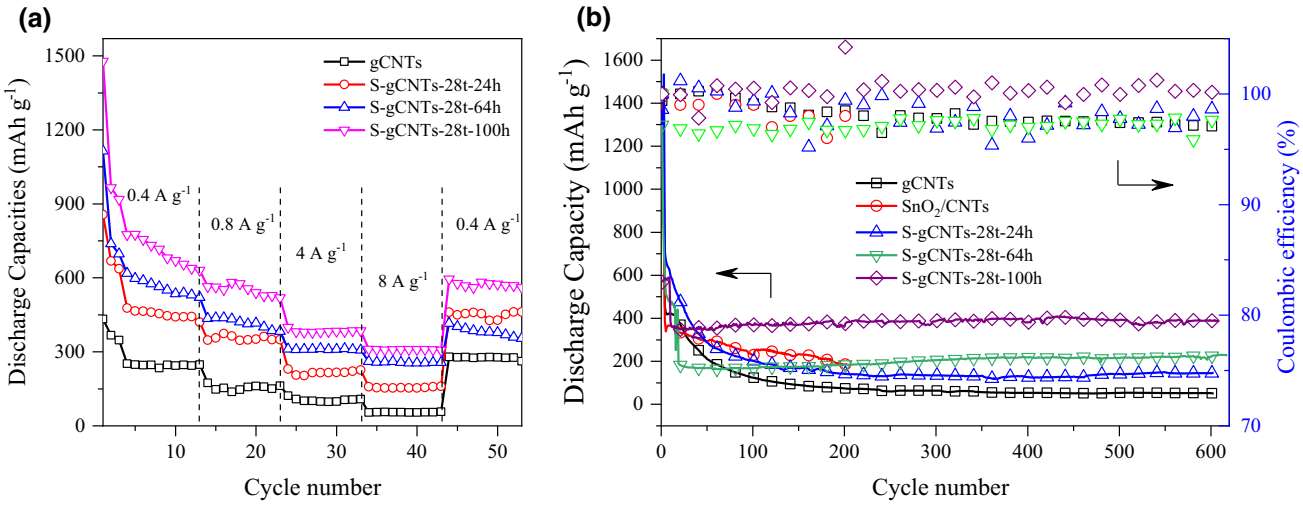

Fig. 6. Electrochemical performance of the samples S-gCNTs-28t-24h, S-gCNTs-28t-64h and S-gCNTs-28t-100h. (a) Rate capabilities at different current density; (b) long-cycle performance at current density of 4 A g^{-1}.

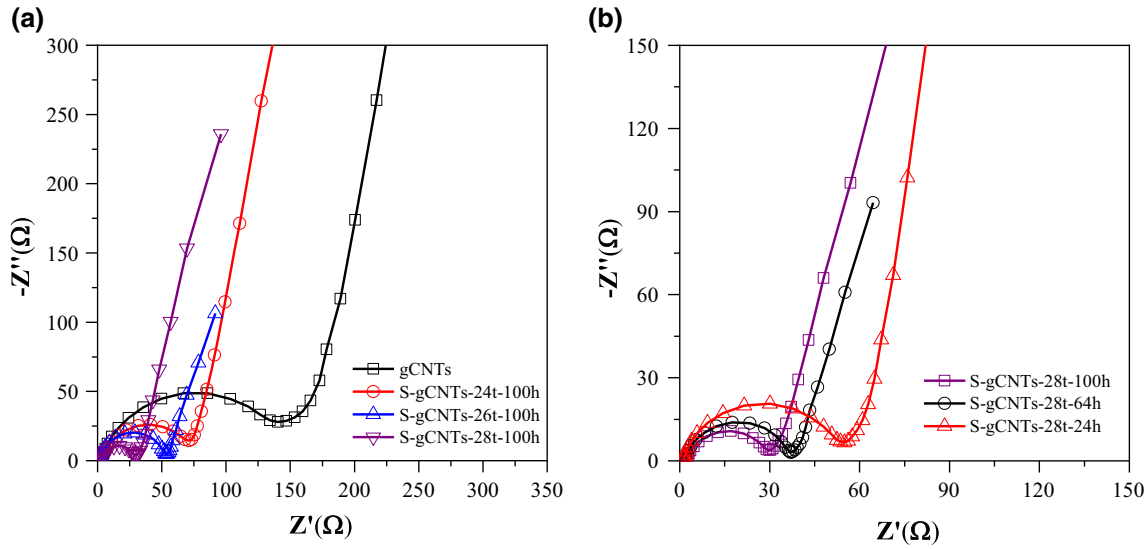

Fig. 7. EIS curves of samples graphited at different temperature (a) and samples with different filling time (b).

CONCLUSIONS

SnO_2/CNT composites for the anode material of LIBs were prepared. CNTs were graphited at high temperature (2400–2800°C) to move the hydrophilic functional group and cause most of the SnO_2 nanoparticles to filled into the cavity of CNTs. Time is the most important role affecting the weight rate of SnO_2 in the composites. The longer the time, the greater the weight of SnO_2 in the composites. S-gCNTs-28t-100h showed the best electrochemical performance in all of samples. It can release a very high stable discharge capacity of 631 mAh g^{-1} at the current density of 0.4 mA g^{-1}. Even at the current density of 8 A g^{-1}, S-gCNTs-28t-100h also released a satisfactory discharge capacity of 308 mAh g^{-1}. Not only that, S-gCNTs composites such as S-gCNTs-28t-100h show a long cycle life, and it can retain a reversible discharge of 383 mAh g^{-1} at current density of 4 A g^{-1} after 620 cycles. The impressive electrochemical performance of the composites can be attributed to the protection of CNTs. Moreover, this work provided a simple and effective strategy to prepare ultrafine nanoparticles encapsulated in carbon nanotubes for anode materials of LIBs.

ACKNOWLEDGMENTS

This work was supported by National Natural Science Foundation of China (Grant Nos. 51662029, 21863006 and 21365013).

REFERENCES

1. Y. Zhao, L. Yang, D. Liu, J. Hu, L. Han, Z. Wang, and F. Pan, *ACS Appl. Mater. Inter.* 10, 1672 (2018).

2. H. Wu, G. Zheng, N. Liu, T.J. Carney, Y. Yang, and Y. Cui, *Nano Lett.* 12, 904 (2012).
3. G. Zhou, K. Liu, Y. Fan, M. Yuan, B. Liu, W. Liu, F. Shi, Y. Liu, W. Chen, J. Lopez, D. Zhuo, J. Zhao, Y. Tsao, X. Huang, Q. Zhang, and Y. Cui, *ACS Cent. Sci.* 4, 260 (2018).
4. S. Qu, Y. Sun, L. Liu, C. Li, C. Yu, X. Zhang, and Y. Chen, *Sci. Rep. UK* 7, 42772 (2017).
5. G. Zhu, Z. He, J. Chen, J. Zhao, X. Feng, Y. Ma, Q. Fan, L. Wang, and W. Huang, *Nanoscale* 6, 1079 (2014).
6. Q.F. Dong, C.Z. Wu, M.G. Jin, Z.C. Huang, M.S. Zheng, J.K. You, and Z.G. Lin, *Solid State Ionics* 167, 49 (2004).
7. C. Kim, J. Jung, K.R. Yoon, D. Youn, S. Park, and I. Kim, *ACS Nano* 10, 11317 (2016).
8. K. Zhao, L. Zhang, R. Xia, Y. Dong, W. Xu, C. Niu, L. He, M. Yan, L. Qu, and L. Mai, *Small* 12, 588 (2016).
9. M. He, L. Yuan, X. Hu, W. Zhang, J. Shu, and Y. Huang, *Nanoscale* 5, 3298 (2013).
10. W. Deng, X. Chen, Z. Liu, A. Hu, Q. Tang, Z. Li, and Y. Xiong, *J. Power Sources* 277, 131 (2015).
11. L. Su, Y. Xu, J. Xie, L. Wang, and Y. Wang, *ACS Appl. Mater. Inter.* 8, 35172 (2016).
12. S. Chen, Y. Xin, Y. Zhou, F. Zhang, Y. Ma, H. Zhou, and L. Qi, *J. Mater. Chem. A* 2, 15582 (2014).
13. M. Wang, H. Yang, X. Zhou, W. Shi, Z. Zhou, and P. Cheng, *Chem. Commun.* 52, 717 (2016).
14. W. Zhou, J. Wang, F. Zhang, S. Liu, J. Wang, D. Yina, and L. Wang, *Chem. Commun.* 51, 3660 (2015).
15. R. Shen, Y. Hong, J.J. Stankovich, Z. Wang, S. Dai, and X. Jin, *J. Mater. Chem. A* 3, 17635 (2015).
16. J. Liu, Y. Li, X. Huang, R. Ding, Y. Hu, J. Jiang, and L. Liao, *J. Mater. Chem.* 19, 1859 (2009).
17. S.H. Choi and Y.C. Kang, *Nanoscale* 5, 4662 (2013).
18. C. Wang, Y. Zhou, M. Ge, X. Xu, Z. Zhang, and J.Z. Jiang, *J. Am. Chem. Soc.* 132, 46 (2010).
19. C. Wang, G. Du, K. Stahl, H. Huang, Y. Zhong, and J.Z. Jiang, *J. Phys. Chem. C* 116, 4000 (2012).
20. H.B. Wu, J.S. Chen, X.W.D. Lou, and H.H. Hng, *J. Phys. Chem. C* 115, 24605 (2011).
21. H. Wang, Q. Liang, W. Wang, Y. An, J. Li, and L. Guo, *Cryst. Growth Des.* 11, 2942 (2011).
22. G.D. Park, J. Lee, and Y.C. Kang, *Adv. Funct. Mater.* 27, 1603399 (2017).
23. R. Jin, Y. Guan, H. Liu, J. Zhou, and G. Chen, *ChemPlusChem* 79, 1643 (2014).
24. H. Guo, R. Mao, D. Tian, W. Wang, D. Zhao, X. Yang, and S. Wang, *J. Mater. Chem. A* 1, 3652 (2013).
25. Z. Lu and H. Wang, *CrystEngComm* 16, 550 (2014).
26. M. Wang, S. Li, Y. Zhang, and J. Huang, *Chem.-Eur. J.* 21, 16195 (2015).
27. L. Li, A. Kovalchuk, and J.M. Tour, *Nano Res.* 7, 1319 (2014).
28. X. Li, X. Zhang, Y. Zhao, D. Feng, Z. Su, and Y. Zhang, *Electrochim. Acta* 191, 215 (2016).
29. L. Zhang, G. Zhang, H.B. Wu, L. Yu, and X.W.D. Lou, *Adv. Mater.* 25, 2589 (2013).
30. Q. Liu, Y. Dou, B. Ruan, Z. Sun, S. Chou, and S.X. Dou, *Chem.-Eur. J.* 22, 5853 (2016).
31. F. Wang, H. Jiao, E. He, S. Yang, Y. Chen, M. Zhao, and X. Song, *J. Power Sources* 326, 78 (2016).
32. D. Liu, Z. Kong, X. Liu, A. Fu, Y. Wang, Y. Guo, P. Guo, H. Li, and X.S. Zhao, *ACS Appl. Mater. Inter.* 10, 2515 (2018).
33. S.H. Choi, J. Lee, and Y.C. Kang, *ACS Nano* 9, 10173 (2015).
34. R. Jin, Y. Meng, and G. Li, *Appl. Surf. Sci.* 423, 476 (2017).
35. R. Liu, D. Li, C. Wang, N. Li, Q. Li, X. Lu, J.S. Spendelow, and G. Wu, *Nano Energy* 6, 73 (2014).
36. D. Liu, Z. Yang, P. Wang, F. Li, D. Wang, and D. He, *Nanoscale* 5, 1917 (2013).
37. Y. Yu, L. Gu, C. Wang, A. Dhanabalan, P.A. van Aken, and J. Maier, *Angew. Chem. Int. Edit.* 48, 6485 (2009).
38. R. Hu, W. Sun, H. Liu, M. Zeng, and M. Zhu, *Nanoscale* 5, 11971 (2013).
39. G. Du, C. Zhong, P. Zhang, Z. Guo, Z. Chen, and H. Liu, *Electrochim. Acta* 55, 2582 (2010).
40. G. An, N. Na, X. Zhang, Z. Miao, S. Miao, K. Ding, and Z. Liu, *Nanotechnology* 18, 435707 (2007).
41. H. Zhang, H. Song, X. Chen, J. Zhou, and H. Zhang, *Electrochim. Acta* 59, 160 (2012).
42. Y. Fu, R. Ma, Y. Shu, Z. Cao, and X. Ma, *Mater. Lett.* 63, 1946 (2009).
43. N.A. Kaskhedikar and J. Maier, *Adv. Mater.* 21, 2664 (2009).
44. S. Yang, W. Yue, J. Zhu, Y. Ren, and X. Yang, *Adv. Funct. Mater.* 23, 3570 (2013).
45. S. Yang, H. Song, H. Yi, W. Liu, H. Zhang, and X. Chen, *Electrochim. Acta* 55, 521 (2009).